Effect of Water Density on Hydrogen Peroxide Dissociation in Supercritical Water. 2. Reaction Kinetics

Naoko Akiya and Phillip E. Savage*

Department of Chemical Engineering, University of Michigan, Ann Arbor, Michigan 48109-2136

Received: June 23, 1999; In Final Form: December 3, 1999

We performed density functional theory (DFT) calculations and molecular dynamics simulations to determine how water influences the kinetics of H_2O_2 dissociation ($H_2O_2 = 2OH$) in supercritical water (SCW). We assumed that the reaction mechanism in SCW is identical to that in the gas phase. We generated the gas-phase potential energy surface for H_2O_2 dissociation by DFT calculations and thereby determined the reactant geometry and partial charges as functions of the oxygen−oxygen separation distance, which we chose to be the reaction coordinate. From the results of these calculations, we postulated the structure of the transition state (TS) for H_2O_2 dissociation. We next conducted two sets of molecular dynamics simulations at $T_r = 1.15$. The first were simulations of dilute solutions of the TS in water, from which we calculated the partial molar volumes for the TS in water. We used these partial molar volumes for the TS and those determined for H_2O_2 from the preceding study to calculate the activation volume for H_2O_2 dissociation in SCW, which in turn provided the density dependence of the rate constant. The results show that the rate constant at $T_r = 1.15$ increases by about 12% as the reduced density of water (ρ_r) increases from 0.25 to 0.75. Between $0.75 < \rho_r < 1.25$, the rate constant is insensitive to changes in density. As the water density increases further to $\rho_r = 2.75$, the rate constant decreases by about 40%. The second set of simulations calculated the change in free energy of solvation along the reaction coordinate for H_2O_2 dissociation at $T_r = 1.15$ and $\rho_r = 1.25$. These simulations revealed that the energy barrier for H_2O_2 dissociation is 2.1 kJ/mol lower in SCW than in the gas phase. This difference in the activation barrier results in the rate constant at $T_r = 1.15$ for H_2O_2 dissociation in SCW being 1.4 times higher than the high-pressure rate constant in the gas phase. The key results from the present study are that the rate constant goes through a maximum with increasing water density and that the rate constant in SCW is larger than the rate constant in the gas phase. Both of these results are consistent with the limited experimental data for this reaction in SCW.

1. Introduction

Oxidation of organic compounds in supercritical water (SCW) is a means of waste treatment and chemical synthesis. H_2O_2 is formed during supercritical water oxidation (SCWO), and its dissociation into highly reactive OH radicals is one of the most important elementary reaction steps in the mechanism. A recent experimental study of H_2O_2 dissociation in SCW indicated that SCW influences the kinetics of this reaction.[1] The rate constant for this reaction in SCW is not only pressure dependent (see Figure 1 in the preceding paper[2]) but also higher than that for the gas-phase reaction at the high-pressure limit based on RRKM (Rice−Ramsperger−Kassel−Marcus) calculations. This pressure dependence and the difference between SCW and gas-phase rate constants suggest that the kinetics of H_2O_2 dissociation is affected by the presence of water in a way that cannot be accounted for by gas-phase kinetics models. This demonstrated effect of water in H_2O_2 dissociation is both scientifically interesting and technologically significant. The rate of this one elementary reaction has a tremendous influence on global SCW oxidation rates. These considerations motivated our molecular simulation study of H_2O_2 dissociation in SCW.

In the preceding paper[2] we used Kirkwood−Buff theory[3] combined with molecular dynamics simulations and density functional theory (DFT) calculations to determine the effect of water density on the reaction equilibrium constant for H_2O_2 dissociation in SCW. In the present article we report results from a molecular dynamics simulation study to elucidate the role of water in the reaction kinetics of H_2O_2 dissociation in SCW. We assumed that the reaction mechanism for H_2O_2 dissociation in SCW is identical to that in the gas phase. We quantified the effect of water density on the rate constant by determining the activation volume. We also quantified the effect of solvation on the activation of H_2O_2 dissociation by calculating the changes in the free energy of solvation along the gas-phase minimum energy path. DFT calculations were conducted to study the gas-phase reaction and to obtain information needed to conduct both sets of simulations. Both the density effect on the rate constant and the solvation effect on the activation can be characterized within the framework of conventional transition state theory, which is a convenient and proven tool for describing the kinetics of an elementary reaction. This approach of immersing the gas-phase reaction system in SCW to quantify the solvent effect was used previously by Melius et al. to study the water gas shift reaction.[4] These authors used an equation of state to calculate the activation volume and the solvent contribution to the free energy of activation, whereas we used molecular simulation in the present study.

* Corresponding author. E-mail: psavage@umich.edu.

10.1021/jp9921001 CCC: $19.00
Published on Web 04/15/2000

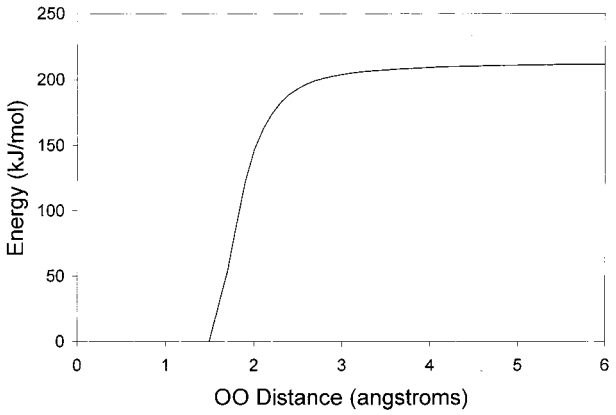

Figure 1. Gas-phase reaction energy for H_2O_2 dissociation.

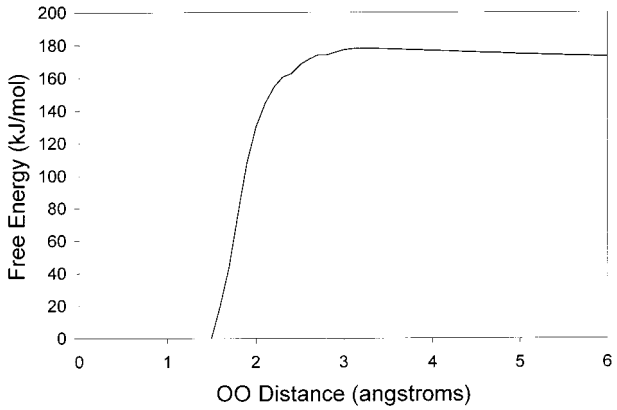

Figure 2. Gas-phase reaction free energy for H_2O_2 dissociation.

1.1. Solvation Effects on Activation. For an elementary reaction, the rate constant (k) derived from transition state theory is

$$k = \kappa\left(\frac{k_B T}{h}\right)\exp\left(\frac{-\Delta G^{\ddagger}}{RT}\right) \tag{1}$$

where κ is the transmission coefficient, k_B is the Boltzmann constant, h is the Planck constant, and $\Delta G^{\ddagger}$ is the free energy of activation.[5] When a chemical reaction takes place in a gas phase, the free energy barrier is completely determined by the interactions among the reactants. When a reaction takes place in solution, however, the free energy barrier is also influenced by the forces exerted by the solvent molecules. In our treatment of solvent effects, we examine the case wherein the solvent system is always equilibrated with the reaction system at all points along the reaction coordinate, and we assume that conventional transition state theory adequately describes the reaction. That is, we will account only for the solvent-induced modifications to the gas-phase free energy profile along the reaction coordinate. This type of solvent effect is referred to as the equilibrium solvation effect. We do not consider possible solvent-induced modifications to the transmission coefficient.[6] Such effects, termed nonequilibrium solvation effects, are outside the scope of this report.

The equilibrium solvation effect can be quantified in terms of the potential of mean force, which is the reversible work needed to bring two reactants in solution from infinite separation to a separation r in the presence of the solvent. The potential of mean force $W(r)$ has two contributions:

$$W(r) = \Delta A_{sol}(r) + \Delta E_{gas}(r) \tag{2}$$

where r represents the reaction coordinate, $\Delta A_{sol}(r)$ is the change in free energy due to the presence of the solvent, and $\Delta E_{gas}(r)$ is the corresponding gas-phase reaction energy. We used the Helmholtz free energy instead of the Gibbs free energy since the simulations were conducted in a canonical ensemble (see section 3.2).

The potential of mean force is an equilibrium quantity calculated for fixed separation distances between the reacting molecules and averaged over equilibrium distributions of solvent molecules. In other words, the potential of mean force incorporates the direct interaction between the reactants and the indirect effective interaction due to the solvent.[7] In terms of the potential of mean force, the rate constant for a reaction in solution (k_s) becomes

$$k_s = \kappa\frac{k_B T}{h}\exp\left(\frac{-W(r^{\ddagger})}{RT}\right) \tag{3}$$

where $r^{\ddagger}$ represents the value of the reaction coordinate at the transition state. If a change in the potential of mean force is the only outcome of transferring a reaction from the gas-phase to solution, the rate constant for the solution-phase reaction can be rewritten in terms of the gas-phase rate constant (k_g):[7]

$$k_s = k_g \exp\left(\frac{-\Delta A_{sol}(r^{\ddagger})}{RT}\right) \tag{4}$$

Thus the change in the free energy of solvation can be used to measure the effect of the solvent on the activation of a reaction.

1.2. Effect of Density on Rate Constant. In conventional transition state theory, the density (ρ) dependence of a rate constant is related to the activation volume ($\Delta v^{\ddagger}$) by[8]

$$\left(\frac{\partial \ln k}{\partial \rho}\right)_T = \frac{1}{\rho\kappa_T}\left\{-\frac{\Delta v^{\ddagger}}{RT} + \left(\frac{\partial \ln \kappa}{\partial P}\right)_T + \kappa_T\left(1 - \sum_{react}\nu_i\right)\right\} \tag{5}$$

where κ_T is the isothermal compressibility of the solvent, and $\sum_{react}\nu_i$ is the sum of the stoichiometric coefficients of the reactants. For unimolecular reactions, such as the one considered here, this sum is 1, so the last term in brackets is equal to zero. Further, we are considering only the equilibrium solvation effects in this study, so the second term in brackets will be neglected. Therefore, for H_2O_2 dissociation SCW, eq 5 simplifies to

$$\left(\frac{\partial \ln k}{\partial \rho}\right)_T = -\frac{\Delta v^{\ddagger}}{\rho RT\kappa_T} \tag{6}$$

The activation volume is calculated as the difference in the partial molar volumes of the transition state ("TS") and the reactant (H_2O_2):

$$\Delta v^{\ddagger} = \bar{v}_{TS} - \bar{v}_{H_2O_2} \tag{7}$$

As we did in the preceding paper,[2] we will use Kirkwood–Buff theory[3] to calculate the partial molar volumes from the pair correlation functions for infinitely dilute mixtures.

2. Gas-Phase Reaction

To use molecular dynamics simulations to determine $\bar{v}_{TS}$ and $\Delta A_{sol}(r)$, one needs a model that describes the potential energy

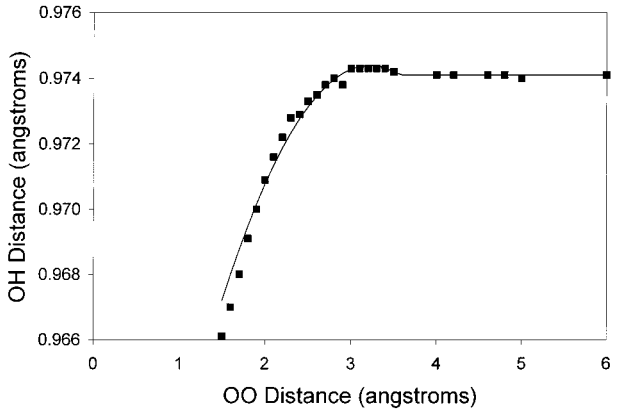

Figure 3. Changes in OH bond distance during H_2O_2 dissociation. DFT data points (■) are fitted using eq 8 (—).

TABLE 1: Bond Dissociation Energies for H_2O_2 Dissociation

energy (kJ/mol)	method	ref
212	B3LYP/6-311+G(3df,2p)	this study
190	PMP2/6-31G(d)	15
209	G2MP2	16
205	G2	16
206	CBSQ	16
204	exptl	17

surface of H_2O_2 as it dissociates. Since we assume that the reaction mechanism of H_2O_2 dissociation in SCW is identical to that in the gas phase, a potential model based on the gas-phase reaction will suffice. Therefore, we performed DFT calculations for an isolated H_2O_2 molecule to obtain the gas-phase reaction energy profile for H_2O_2 dissociation. We constructed the reaction energy profile by conducting a series of partial geometry optimizations along an assumed reaction coordinate followed by thermochemistry calculations and atomic charge analysis. We chose the oxygen−oxygen (OO) separation distance as the reaction coordinate and fixed it to a desired value during each partial geometry optimization routine. To describe the changes in the energy, geometry, and partial charges of an isolated H_2O_2 molecule as it dissociates, we took the simplest approach, which is to make these quantities a function of only the reaction coordinate (see for example ref 9). The energy and geometry profiles were used to postulate the structure of the transition state. As in the preceding paper, we used the B3LYP functional[10−12] with the 6-311+G(3df,2p) basis set for all calculations. We used the CHelpG method[13] to calculate partial atomic charges for H_2O_2. All calculations were performed by Gaussian 94, Revision B.3.[14] The balance of this section provides more details regarding these DFT calculations.

Figure 1 shows the reaction energy profile for H_2O_2 dissociation in the gas phase. The reaction energy profile lacks a saddle point and hence reveals no obvious transition state, which is consistent with a previous computational study.[15] The free energy profile obtained from thermochemical calculations (Figure 2), on the other hand, shows a small maximum near $r_{OO} = 3$ Å. Table 1 compares the bond dissociation energy we calculated with those from previous theoretical and experimental studies.[15−17] This comparison suggests that B3LYP/6-311+G(3df,2p) is adequate for describing H_2O_2 dissociation.

Figures 3−5 show the changes in the OH bond length, the HOO angle, and HOOH dihedral angle, respectively, with changes in the OO distance, and Figure 6 provides a schematic representation of these geometry changes. There are marked changes in molecular geometry between $r_{OO} = 1.4464$ Å (the equilibrium distance) and 2.5−3 Å. As the OO distance begins

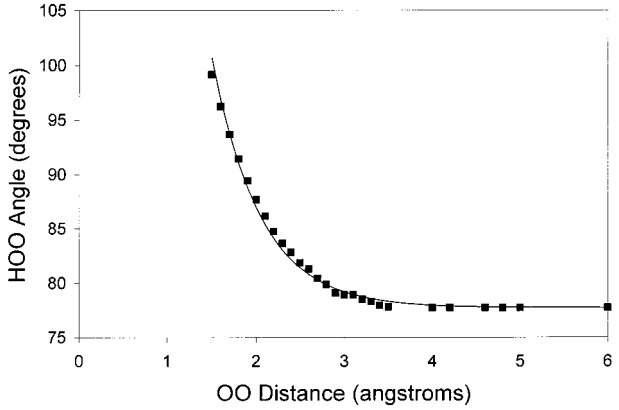

Figure 4. Changes in HOO angle during H_2O_2 dissociation. DFT data points (■) are fitted using eq 9 (—).

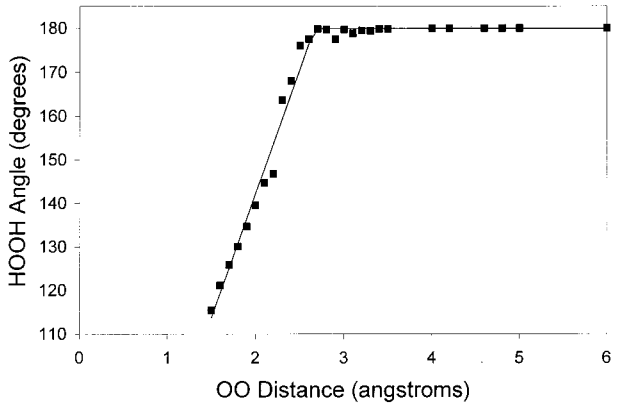

Figure 5. Changes in HOOH angle during H_2O_2 dissociation. DFT data points (■) are fitted using eq 10 (—).

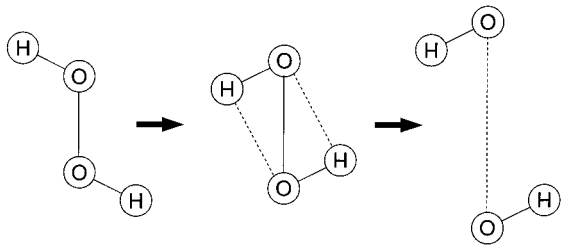

Figure 6. Changes in geometry during H_2O_2 dissociation.

TABLE 2: Geometries of the Reactant and Transition State for H_2O_2 Dissociation

geometry	H_2O_2	TS
r_{OO} (Å)	1.4464	3.0000
r_{OH} (Å)	0.9659	0.9743
∠HOO (deg)	100.8982	78.9222
∠HOOH (deg)	111.9324	179.6744

to increase, the HOO angle becomes smaller and the structure becomes more planar. This change in geometry also reduces the distance between an oxygen atom and the hydrogen atom to which it is not bonded. Beyond $r_{OO} = 3$ Å, however, there is very little change in molecular geometry except the lengthening of the OO bond. In other words, the OH groups become farther apart from each other with little change in their orientation. Considering these changes in geometry as well as the location of the maximum in the free energy profile, we chose the geometry at $r_{OO} = 3$ Å to approximate the transition state structure for H_2O_2 dissociation. Table 2 summarizes the geometries of the reactant and the transition state.

Figure 7 shows the changes in the partial charge on a

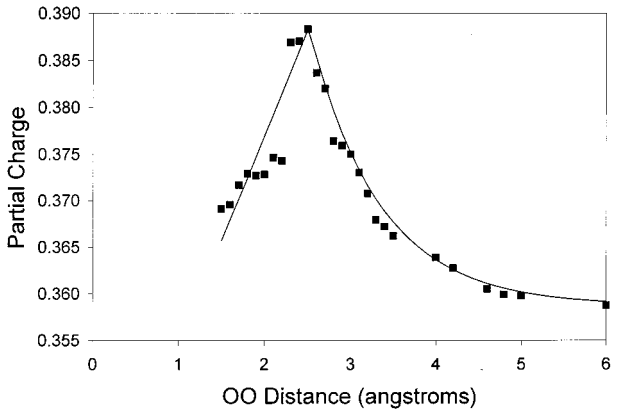

Figure 7. Changes in partial charges during H_2O_2 dissociation. DFT data points (■) are fitted using eq 11 (—).

hydrogen atom along the reaction coordinate. The corresponding partial charge on an oxygen atom is equal to the values shown for hydrogen but of opposite sign ($q_H = -q_O$). The variation of the partial charge along the reaction coordinate is small (between 0.36 and 0.39), but there is clearly a sharp maximum at $r_{OO} = 2.5$ Å. This behavior must be associated with the way the H_2O_2 geometry changes along the reaction coordinate, which was shown schematically in Figure 6.

The DFT calculations provided the molecular geometry and partial charges at discrete points along the reaction coordinate. We fit these data to continuous analytical functions of only the OO distance for convenience in the subsequent molecular simulations.

$$r_{OH} = \begin{cases} -2.4447 \times 10^{-3}\, r_{OO}^2 + 1.5720 \times 10^{-2}\, r_{OO} + 9.4913 \times 10^{-1} & r_{OO} \le 3.5\ \text{Å} \\ 0.9741 & r > 3.5\ \text{Å} \end{cases} \quad (8)$$

$$\theta_{HOO} = 0.031 \exp[-1.83(r_{OO} - 5.11)] + 77.73 \quad (9)$$

$$\phi_{HOOH} = \begin{cases} 57.1554 r_{OO} + 27.9999 & r_{OO} \le 2.6577\ \text{Å} \\ 179.9 & r_{OO} > 2.6577\ \text{Å} \end{cases} \quad (10)$$

$$q_H = -q_O = \begin{cases} 0.0226 r_{OO} + 0.3318 & r_{OO} \le 2.5\ \text{Å} \\ 0.03 \exp[-1.2(r_{OO} - 2.5)] + 0.3587 & r_{OO} > 2.5\ \text{Å} \end{cases} \quad (11)$$

These functions are plotted along with the DFT data in Figures 3 − 5 and 7. These functions were used instead of the discrete data points to calculate the geometry and partial charges of H_2O_2 at a specified value of the OO distance during the free energy calculations.

3. Molecular Dynamics Simulation

We performed molecular dynamics simulations to calculate two key quantities. One is the partial molar volume of the transition state species from which we can then calculate the activation volume for H_2O_2 dissociation in SCW. The second quantity is the change in free energy of solvation along the reaction coordinate. This quantity allows us to compare the rates of H_2O_2 dissociation in the gas phase and in SCW. This section provides some details regarding these molecular dynamics simulations.

3.1. Potential Models. In the preceding paper[2] we summarized the development of the intermolecular potential model that describes both H_2O_2−water interactions and OH−water interactions. This potential model is based on the DFT potential energy surface for H_2O_2−water and OH−water dimers. We used this same potential model to describe the TS−water interactions for the present simulations. The intermolecular potential contains electrostatic and Lennard-Jones terms:

$$V_{mn} = \sum_i^m \sum_j^n \left\{ \frac{q_i q_j}{4\pi\epsilon_0 r_{ij}} + \frac{A_{ij}}{r_{ij}^{12}} - \frac{B_{ij}}{r_{ij}^{6}} \right\} \quad (12)$$

The indices i and j refer to atomic sites on molecules m and n, and r_{ij} is the distance between sites i and j. The parameters A_{ij} and B_{ij} retained the same values used previously[2] to describe H_2O_2−water and OH−water interactions. These parameters were held constant in all simulations. Partial charges (q_i, q_j), on the other hand, were varied with the reaction coordinate according to eq 11. As in the preceding work, we used the TJE model[18] to describe the intermolecular and intramolecular potentials of water.

3.2. Simulation Procedures. The system used to calculate the partial molar volume of the transition state species comprised a single transition state structure for H_2O_2 dissociation in a simulation box with 499 water molecules (i.e., mole fraction = 0.002). The simulations were conducted at a reduced temperature of $T_r = 1.15$ and reduced densities of $\rho_r = 0.25$, 0.33, 0.42, 0.50, 0.75, 0.88, 1.12, 1.25, 1.75, 2.25, and 2.75. These reduced properties are based on the reported critical properties for TJE water.[19] These simulation conditions are identical to those used in our previous study[2] to calculate the reaction volume for H_2O_2 dissociation. For each simulation, we equilibrated the system for at least 400 ps and accumulated data for 1.8 ns.

The system used to calculate the changes in the free energy of solvation initially comprised a single H_2O_2 molecule at its equilibrium geometry $r_{OO} = 1.4464$ Å in a simulation box of 499 water molecules. We used the perturbation method[20] to calculate the incremental change in the free energy of solvation along the reaction coordinate for H_2O_2 dissociation:

$$\delta A(r) = -k_B T \left\langle \frac{\exp[V_{UV}(r + \delta r) - V_{UV}(r)]}{k_B T} \right\rangle_r \quad (13)$$

where r is the reaction coordinate and V_{UV} is the solute−solvent interaction energy. Here $\delta A(r)$ is the change in free energy of solvation when the OO separation distance is perturbed from r to $r + \delta r$. The brackets indicate a configurational average evaluated over the ensemble representative of the specified point along the reaction coordinate. The range of the OO separation distance of interest is from its equilibrium value for H_2O_2 (1.4464 Å) to 6 Å, beyond which H_2O_2 resembles two distinct OH groups. This total range was divided into 34 windows of size δr ($\delta r = 0.1$ Å for $r_{OO} \le 3.4$ Å, $\delta r = 0.2$ Å for $r_{OO} > 3.4$ Å) that were sufficiently small to ensure the numerical accuracy of eq 13. The system was perturbed in both forward and backward directions to obtain two values of the free energy change per window, except for the end windows. The values reported are the means of the forward and backward results. The geometry and partial charges of H_2O_2 were changed from window to window according to eqs 8−11 to model dissociation. The simulations were conducted at a reduced temperature of $T_r = 1.15$ and a reduced density of $\rho_r = 1.25$. The starting configuration was equilibrated for 500 ps. Subsequent simulations were conducted successively along the reaction coordinate. At each value of r_{OO} the system was equilibrated for 10 ps and

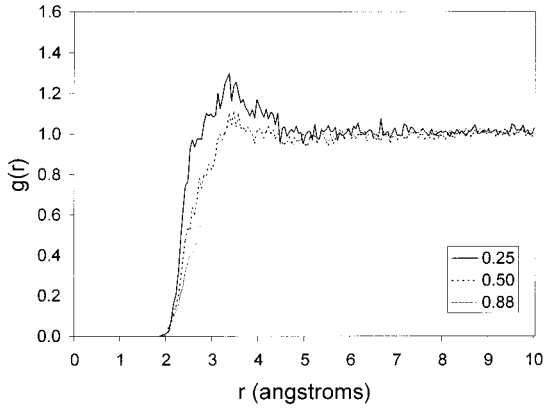

Figure 8. TS−water pair correlation functions at $T_r = 1.15$ and $\rho_r = 0.25$, 0.50, and 0.88.

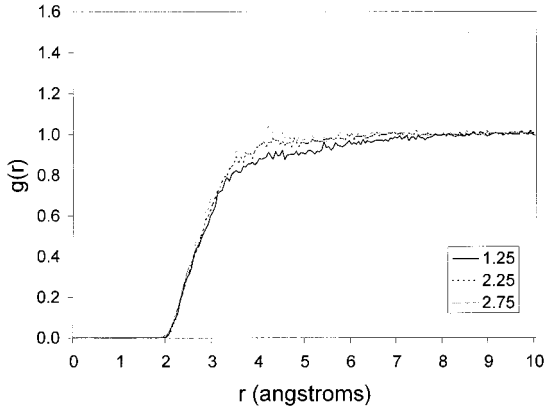

Figure 9. TS−water pair correlation functions at $T_r = 1.15$ and $\rho_r = 1.25$, 2.25, and 2.75.

perturbed by δr for 40 ps. The total simulation length, including equilibration, was 2.19 ns.

All simulations were conducted in a canonical ensemble (*NVT*). We used the reversible reference system propagator algorithm (r-RESPA)[21,22] to integrate the equations of motion. We took the long time step to be 1 fs and the short time step to be 0.1 fs for all simulations. The Nosé−Hoover method[23,24] was used for temperature control to ensure that a canonical ensemble was obtained. The method was implemented with a single thermostat with a fluctuation period of 10 fs. The solute geometry was kept rigid using the RATTLE algorithm.[25]

Standard simulation procedures, including the Verlet neighbor list, periodic boundary conditions, and the minimum image conventions, were used.[26,27] All interactions were truncated at 10 Å. The long-range electrostatic interactions were treated with the reaction field method.[26,28] The dielectric constant of the dielectric continuum, ϵ_{RF} was chosen to be 80, as any value of ϵ_{RF} between the value of the true dielectric constant and infinity is acceptable for moderately and highly polar substances.[28] The dielectric constant of SCW is lower than that of ambient water, which is about 80.

4. Results and Discussion

4.1. Density Effects. *4.1.1. Structural Properties.* Figures 8 and 9 show the solute−solvent pair correlation functions for water molecules around the transition state (TS) for $H_2O_2 =$ 2OH. The correlations were determined from center-of-mass separation distances. We sampled pair correlation functions every 50 fs using a sampling bin width of 0.5 Å. The correlations for subcritical and supercritical water densities are shown separately for clarity. These figures show that the pair correlation functions exhibit different density dependences at subcritical and supercritical densities. Below the critical density of TJE water, the peak height decreases with increasing density. On the other hand, above the critical density, the peak height increases with increasing density. These trends are consistent with those observed for H_2O_2 and OH in TJE water and suggest that the relative strengths of TS−water and water−water interactions are sensitive to changes in water density, as reported in the previous paper.[2]

The shape of the TS−water pair correlation functions is different from that of H_2O_2−water pair correlation functions (see Figures 4 and 5 in the previous paper). There are two major differences. First, the center-of-mass separation distance at which the TS−water pair correlation functions first become nonzero (∼2.0 Å) is smaller than that for H_2O_2−water pair correlation functions (∼2.3 Å). Second, the H_2O_2−water pair correlation functions show a sharper peak, which indicates a more clearly defined solvent structure around the solute. These differences arise from the different structures of the TS and H_2O_2. Because of the greater distance between the oxygen atoms in the TS, there is more room around the center of mass, and water molecules have greater access to the center of mass of the TS. That is, water molecules can get closer to the center of mass of the TS than that of H_2O_2, despite the larger size of the TS due to OO bond stretching. As a result, the TS−water pair correlation functions have their first nonzero value at a smaller separation distance than the H_2O_2−water pair correlation functions. Although this minimum TS−water separation distance remains constant for all water densities examined, the pair correlation functions increase much more slowly than those for H_2O_2 at higher densities. The TS structure being much more elongated than that of H_2O_2 makes it difficult for the water molecules surrounding the TS to form a radial solvation shell as clearly defined as that around H_2O_2. As a result, the TS−water pair correlation functions have either broad peaks (at low densities) or no peaks at all (at higher densities). These observations suggest that the TS in water is less solvated than H_2O_2 at higher densities.

The partial molar volumes $\bar{v}_U^\infty$ were calculated from Kirkwood−Buff theory[3] using the pair correlation functions $g_{ij}(r)$ according to eqs 14 and 15:

$$\bar{v}_U^\infty = \frac{1}{\rho} - (G_{UV} - G_{VV}) = \frac{1 - N^{ex}}{\rho} \tag{14}$$

$$G_{ij} = 4\pi \int_0^\infty [g_{ij}(r) - 1] r^2 \, dr \tag{15}$$

where N^{ex} in Equation 14 is the number of excess solvent molecules discussed in the previous paper.[2] The integration in eq 15 was carried out to $r = 10$ Å. N^{ex} was calculated at each 200 ps interval during the simulation. Since we had multiple determination of N^{ex} at each state point, we were able to calculate the mean and the standard deviation of N^{ex} for each state point. We determined the uncertainties for all the partial molar volumes and other calculated properties that we report in this paper from the uncertainty for N^{ex} and the propagation of errors formula. Figures 10 and 11 show the number of excess water molecules around TS and the partial molar volume of TS in SCW at various water densities. Both N^{ex} and $\bar{v}_U^\infty$ have a water density dependence similar to that of H_2O_2 and OH in SCW.[2] The results suggest that TS in SCW is also a repulsive mixture,[2,29] i.e., TS−water interactions are less attractive than water−water interactions.

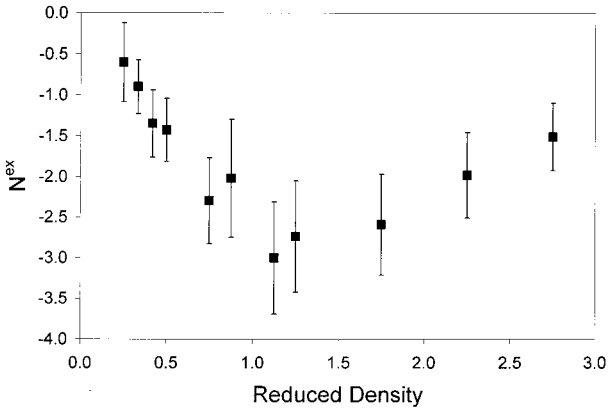

Figure 10. Number of excess solvent molecules for TS in water at $T_r = 1.15$.

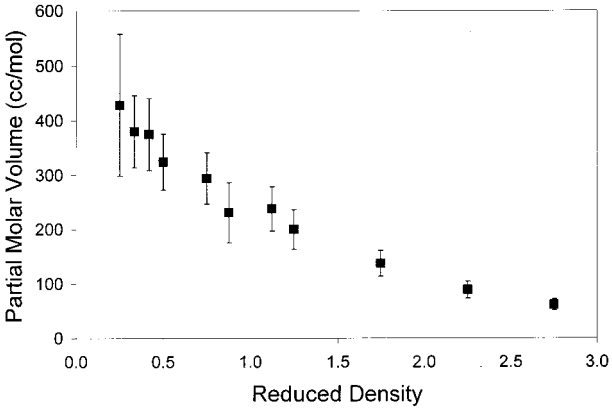

Figure 11. TS partial molar volume in water at $T_r = 1.15$.

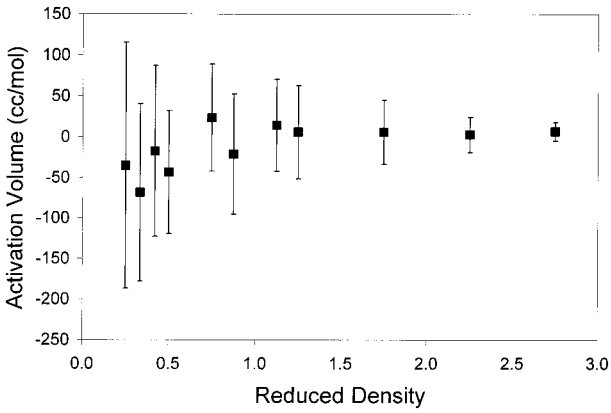

Figure 12. Activation volume for H_2O_2 dissociation in SCW at $T_r = 1.15$.

4.1.2. Density Effects on Reaction Kinetics. The activation volumes in Figure 12 were calculated from the partial molar volumes of the TS and H_2O_2 (from the previous paper[2]) in SCW using eq 7. There is considerable scatter in the calculated values at lower densities, but if the mean values are a reliable indicator, the activation volume undergoes a transition from negative to positive values as the density increases. This transition from negative to positive activation volume with increasing density occurs because the relative solvation of the TS and H_2O_2 in SCW changes with density, as indicated by the comparison of the pair correlation functions for TS−water and H_2O_2−water systems. The significance of preferential solvation in the density effects on rate constants is discussed in depth by Chialvo et al.[30]

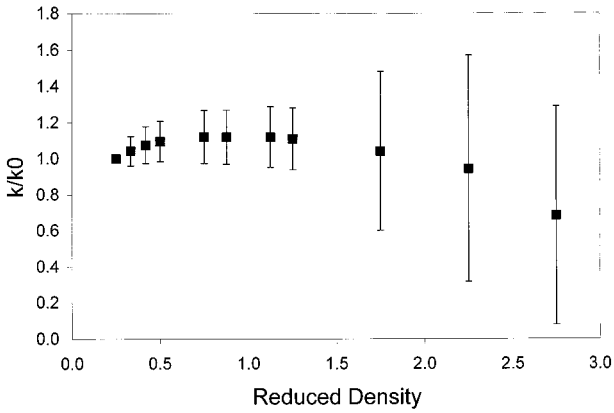

Figure 13. Relative rate constant for H_2O_2 dissociation in SCW at $T_r = 1.15$.

Having determined the activation volume at different water densities, we can now integrate eq 6 to determine the density dependence of the rate constant for H_2O_2 dissociation in SCW at $T_r = 1.15$. According to eq 6, the water density dependence of the rate constant is a function of the water density itself, the isothermal compressibility of water, and the activation volume. Both density and isothermal compressibility are the properties of the solvent. The activation volume accounts for the solute−solvent interactions, and the partial molar volumes from which it is calculated also depend on solvent density and isothermal compressibility, as discussed in the previous section. Therefore, the water density effects that we report here arise from both solute−solvent interactions as well as the bulk solvent properties. We speculate that the effects due to solute−solvent interactions dominate at low densities, while the effects due to bulk solvent properties dominate at high densities.

Figure 13 shows the results of the numerical integration of the relative rate constant as a function of the water density. The rate constant for the lowest density state was arbitrarily chosen as the reference point (k_0). The uncertainty in the rate constant at higher densities ($\rho_r > 1.5$) is large, because the partial derivative of the rate constant with respect to density is inversely proportional to the isothermal compressibility (see eq 6), which becomes very small at these densities. The mean value of the rate constant at $T_r = 1.15$ increases by about 12% as the reduced density of water (ρ_r) increases from 0.25 to 0.75. Between $0.75 < \rho_r < 1.25$, the rate constant is insensitive to changes in density. As the water density increases further to $\rho_r = 2.75$, the rate constant decreases by about 40%. The maximum in the rate constant with increasing water density is due to the transition from negative to positive activation volumes.

The qualitative density dependence in Figure 13 is consistent with the limited experimental data available for H_2O_2 dissociation in SCW. These data show that the rate constant for H_2O_2 dissociation in SCW is higher than the gas-phase rate constant.[1] That is, the rate constant must increase as the water density is increased from zero in the gas-phase to a nonzero value in SCW. On the other hand, the experimental data also show that the rate constant for H_2O_2 dissociation in SCW decreases with increasing water density.[1] For these two trends to be consistent there must be a maximum in the rate constant at an intermediate water density. It is difficult to make a more direct comparison of our results with the experimental data, however, since our simulations were not conducted at the same conditions that were used for the experimental study.

Mechanism-based kinetics models for SCWO are generally constructed from chemical reactions and kinetics parameters drawn from the gas-phase combustion literature. These models

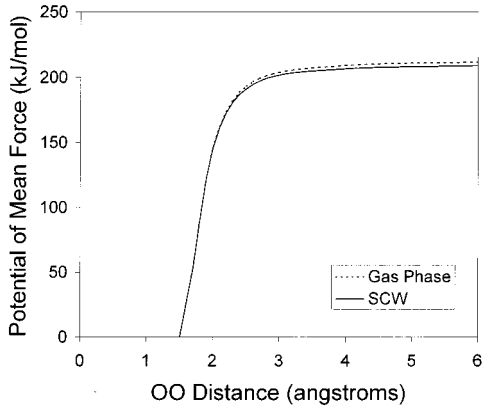

Figure 14. Potential of mean force for H_2O_2 dissociation in SCW at $T_r = 1.15$ and $\rho_r = 1.25$.

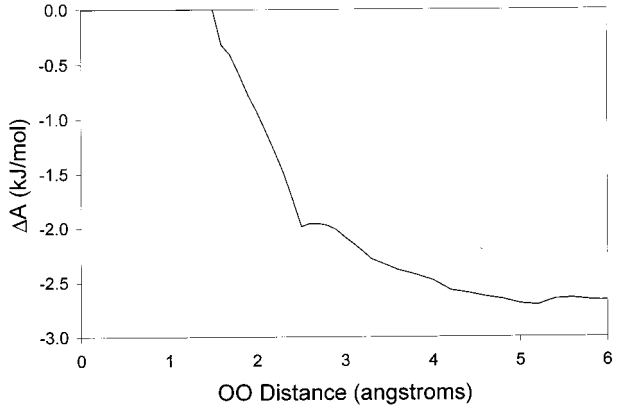

Figure 15. Change in free energy of solvation for H_2O_2 dissociation in SCW at $T_r = 1.15$ and $\rho_r = 1.25$.

do incorporate the effect of water but only by including water as a reactant or a collision partner. Gas-phase reaction models cannot capture physical effects such as solute−solvent interactions and bulk solvent properties, which are responsible for the density effects shown in this study. One can, however, use the computational approach demonstrated in this work to quantify the water density dependence of the rate constant and thus effectively incorporate the water density effects on the SCWO kinetics in mechanism-based kinetics models.

4.2. Potential of Mean Force in Supercritical Water. Figure 14 shows the potential of mean force for H_2O_2 dissociation in water at $T_r = 1.15$ and $\rho_r = 1.25$. The contribution of the free energy of solvation to the potential of mean force is such that there is less than 3.0 kJ/mol difference between the potential of mean force in SCW and the corresponding gas-phase reaction energy profile.

The change in free energy of solvation along the reaction coordinate is plotted separately in Figure 15. The change in free energy of solvation being less than zero indicates that H_2O_2−water interactions become increasingly attractive as the reaction proceeds. This result is consistent with the modest increase in the rate constant with increasing water density at low densities (Figure 13). The change in the free energy of solvation is partially due to the change in the partial charges as H_2O_2 dissociates. We point this out because we believe that the sharp change that appears at $r_{OO} = 2.5$ Å is an artifact from the choice of analytic functions used to describe the dependence of partial charges on the reaction coordinate. Recall from Figure 7 that the magnitude of the partial charge shows a sharp peak at $r_{OO} = 2.5$ Å.

Our results indicate that solvation lowers the activation barrier for H_2O_2 dissociation at $T_r = 1.15$ and $\rho_r = 1.25$ by 2.09 ± 0.012 kJ/mol, where the uncertainty reported is determined from half the hysteresis. The uncertainty per window did not exceed ±0.09 kJ/mol. We can use conventional transition state theory to estimate the change in the rate constant that would result from this much difference in the activation barrier. Assuming that the pre-exponential factor is unaffected, we obtain from eq 4

$$\frac{k_{SCW}}{k_{gas}} = \exp\left(\frac{2.09 \pm 0.012}{RT}\right) = 1.44 \pm 0.003 \qquad (16)$$

which means that for the same reduced temperature and density, the rate constant for H_2O_2 dissociation in SCW is 44% higher than that for the gas-phase reaction. The reduced temperature and density used in our simulations correspond to 744 K and 403 kg/m^3 for real water. Using the experimentally determined Arrhenius parameters for H_2O_2 dissociation in SCW[1] and the recommended parameters for the reaction in the gas phase at high-pressure limit,[31] we calculate the rate constant in SCW to be 3.27 times higher than that in the gas phase at 744 K. If one accounts for the reported uncertainties in the rate constants ($\Delta\log k_{SCW} = 0.1$, $\Delta\log k_{gas} = 0.5$), however, this ratio of the SCW rate constant to the gas-phase rate constant can be as high as 10.6 and as low as 1.01. Since the ratio we calculated from the simulation is consistent with the experimental ratio (considering uncertainty) we conclude that the enhanced rate of H_2O_2 dissociation in SCW is consistent with a solvation-induced reduction in the energy barrier for this reaction. One can thus use the free-energy calculation approach employed in this study to incorporate the solvation effects into the activation barrier and improve the values of the kinetics parameters used in mechanism-based kinetics models.

5. Conclusion

We have elucidated the role of water in the kinetics of H_2O_2 dissociation in SCW at $T_r = 1.15$ by using DFT calculations and molecular dynamics simulations combined with Kirkwood−Buff theory. We quantified the density dependence of the rate constant by calculating the activation volume at $\rho_r = 0.25$−2.75. We also quantified the difference between the activation barriers of the gas-phase and SCW-phase reaction by calculating the changes in the free energy of solvation at $\rho_r = 1.25$ along the reaction coordinate, which we took to be the oxygen−oxygen separation distance of H_2O_2.

The rate constant for H_2O_2 dissociation is a function of the water density. It increases by approximately 12% as the reduced density of water increases from $\rho_r = 0.25$−1, and then it decreases by approximately 40% as the reduced density increases further to $\rho_r = 2.75$. The observed density dependence of the rate constant is qualitatively consistent with available experimental data for H_2O_2 dissociation in SCW.[1]

The activation barrier for H_2O_2 dissociation in SCW is about 2.1 kJ/mol lower than that in the gas phase. This difference translates to a rate constant for H_2O_2 dissociation that is 44% higher in SCW ($T_r = 1.15$, $\rho_r = 1.25$) than in the gas-phase at the high-pressure limit and at the same reduced temperature. The ratio of SCW-phase to gas-phase rate constant that we obtained from simulations agrees with the ratio calculated from the literature rate constants,[1,31] within the published uncertainties.

The present and preceding[2] studies present a systematic approach that can be used to improve mechanism-based kinetics models of SCWO. Generally, the kinetics and thermochemical data for these detailed chemical kinetics models are drawn from

the combustion literature. Applying such gas-phase models to SCWO conditions, however, completely neglects solvent density effects, which arise from the solute−solvent interactions and bulk solvent properties. The present and preceding[2] studies elucidated the density effects on the rate constant and the equilibrium constant for H_2O_2 dissociation. The present study also sheds light on the effect of solvation on the activation of this reaction. Our results indicate that these density and solvation effects influence (by less than an order of magnitude) the kinetics of H_2O_2 dissociation, which is an important step in the overall reaction mechanism of SCWO.

Additionally, the results presented herein show that the changes in solvation along the reaction coordinate and changes in solvation with density are consistent with the experimentally observed effect of water on H_2O_2 dissociation rates in SCW. Given the fact that global SCWO rates are extremely sensitive to the rate of H_2O_2 dissociation, we conclude that one way that changes in the water density influence global SCWO rates is through density-induced changes in the differential solvation of reactants, products, and transition states. Thus, changes in differential solvation must be added to the list of partial and potential causes of water density effects on global SCWO rates. This list includes cage effects,[32,33] water acting as a collision partner and/or a reactant,[34−37] and water molecules interacting with transition states.[38,39]

One must also keep in mind that the bulk solvent properties also play an important role in the observed density dependence of the rate constant and the equilibrium constant. This observation underscores the need to consider the system as a whole when attempting to rationalize the observed water density effects on SCWO kinetics. One must account for changes in the behavior and properties of water as well as those of the solute−water interactions with changing water density.

Acknowledgment. This material is based upon work supported by the National Science Foundation under Grants CTS-9521698 and CTS-9903373 and the Graduate Fellowship. N.A. thanks Prof. Robert Ziff for helpful discussions and Javier Takimoto for technical assistance.

References and Notes

(1) Croiset, E.; Rice, S. F.; Hanush, R. G. *AIChE J.* **1997**, *43*, 2343.
(2) Akiya, N.; Savage, P. E. *J. Phys. Chem. A* **2000**, *104*, 4433.
(3) Kirkwood, J. G.; Buff, F. P. *J. Chem. Phys.* **1951**, *19*, 774.
(4) Melius, C. F.; Bergan, N. E.; Shepherd, J. E. *Proceedings of the International Symposium on Combustion*; Combustion Institute: Pittsburgh, 1990; p 217,
(5) Laidler, K. J. *Chemical Kinetics*, 3rd ed.; Harper Collins: New York, 1987.
(6) van der Zwan, G.; Hynes, J. T. *J. Chem. Phys.* **1983**, *78*, 4174.
(7) Billing, G. D.; Mikkelsen, K. V. *Molecular Dynamics and Chemical Kinetics*; John Wiley and Sons: New York, 1996.
(8) Savage, P. E.; Gopalan, S.; Mizan, T. I.; Martino, C. J.; Brock, E. E. *AIChE J.* **1995**, *41*, 1723.
(9) Chandrasekhar, J.; Smith, S. F.; Jorgensen, W. L. *J. Am. Chem. Soc.* **1985**, *107*, 154.
(10) Becke, A. D. *J. Chem. Phys.* **1993**, *98*, 5648.
(11) Miehlich, B.; Savin, A.; Stoll, H.; Preuss, H. *Chem. Phys. Lett.* **1989**, *157*, 200.
(12) Lee, C. T.; Yang, W. T.; Parr, R. G. *Phys. Rev. B* **1988**, *37*, 785.
(13) Breneman, C. M.; Wiberg, K. B. *J. Comput. Chem.* **1990**, *11*, 361.
(14) Frisch, M. J.; Trucks, G. W.; Schlegel, H. B.; Gill, P. M. W.; Johnson, B. G.; Robb, M. A.; Cheeseman, J. R.; Keith, T.; Petersson, G. A.; Montgomery, J. A.; Raghavachari, K.; Al-Laham, M. A.; Zakrzewski, V. G.; Ortiz, J. V.; Foresman, J. B.; Peng, C. Y.; Ayala, P. Y.; Chen, W.; Wong, M. W.; Andres, J. L.; Replogle, E. S.; Gomperts, R.; Martin, R. L.; Fox, D. J.; Binkley, J. S.; Defrees, D. J.; Baker, J.; Stewart, J. P.; Head-Gordon, M.; Gonzalez, C.; Pople, J. A. *Gaussian94*, Revision B.3; Gaussian: Pittsburgh, 1995.
(15) Benassi, R.; Taddei, F. *Tetrahedron* **1994**, *50*, 4795.
(16) Bach, R. D.; Ayala, P. D.; Schlegel, H. B. *J. Am. Chem. Soc.* **1996**, *118*, 12758.
(17) Luo, X.; Fleming, P. R.; Rizzo, T. R. *J. Chem. Phys.* **1992**, *96*, 5659.
(18) Teleman, O.; Jönsson, B.; Engström, S. *Mol. Phys.* **1987**, *60*, 193.
(19) Mizan, T. I.; Savage, P. E.; Ziff, R. M. *J. Supercrit. Fluids* **1997**, *10*, 119.
(20) Zwanzig, R. W. *J. Chem. Phys.* **1954**, *22*, 1420.
(21) Martyna, G. J.; Tuckerman, M. E.; Tobias, D. J.; Klein, M. L. *Mol. Phys.* **1996**, *87*, 1117.
(22) Tuckerman, M.; Berne, B. J.; Martyna, G. J. *J. Chem. Phys.* **1992**, *97*, 1990.
(23) Hoover, W. G. *Phys. Rev. A* **1985**, *31*, 1695.
(24) Nosé, S. *Mol. Phys.* **1984**, *52*, 255.
(25) Andersen, H. C. *J. Comput. Phys.* **1983**, *52*, 24.
(26) Allen, M. P.; Tildesley, D. J. *Computer Simulation of Liquids*; Oxford University Press: Oxford, 1987.
(27) Haile, J. M. *Molecular Dynamics Simulation: Elementary Methods*; John Wiley and Sons: New York, 1992.
(28) Neumann, M. *J. Chem. Phys.* **1985**, *82*, 5663.
(29) Debenedetti, P. G.; Mohamed, R. S. *J. Chem. Phys.* **1989**, *90*, 4528.
(30) Chialvo, A. A.; Cummings, P. T.; Kalyuzhnyi, Yu. V. *AIChE J.* **1998**, *44*, 667.
(31) Baulch, D. L.; Cobos, C. J.; Cox, R. A.; Frank, P.; Hayman, G.; Just, Th.; Kerr, J. A.; Murrells, T.; Pilling, M. J.; Troe, J.; Walker, R. W.; Warnatz, J. *J. Phys. Chem. Ref. Data* **1994**, *23*, 847.
(32) Yang, H. H.; Eckert, C. A. *Ind. Eng. Chem. Res.* **1988**, *27*, 2009.
(33) Helling, R. K.; Tester, J. W. *Energy Fuels* **1987**, *1*, 417.
(34) Koo, M.; Lee, W. K.; Lee, C. H. *Chem. Eng. Sci.* **1997**, *52*, 1201.
(35) Steeper, R. R.; Rice, S. F.; Kennedy, I. M.; Aiken, J. D. *J. Phys. Chem.* **1996**, *100*, 184.
(36) Holgate, H. R.; Tester, J. W. *J. Phys. Chem.* **1994**, *98*, 800.
(37) Holgate, H. R.; Tester, J. W. *J. Phys. Chem.* **1994**, *98*, 810.
(38) Akiya, N.; Savage, P. E. *AIChE J.* **1998**, *44*, 405.
(39) Rice, S. F.; Steeper, R. R.; Aiken, J. D. *J. Phys. Chem. A* **1998**, *102*, 2673.